MICRO-MECHANICAL MODEL OF A SINGLE CRYSTAL NICKEL-BASED SUPERALLOY

T. Tinga*, M.G.D. Geers, W.A.M. Brekelmans****
***National Aerospace Laboratory NLR, Amsterdam, The Netherlands**
****Eindhoven University of Technology, Eindhoven, The Netherlands**

Keywords: *micromechanics, superalloy, gas turbine*

Abstract

A multi-scale micro-mechanical model for a nickel-base superalloy is presented. The model takes into account the multiphase character of the material and is thus able to predict the effect of microstructure morphology on the macroscopic material response. The model is implemented in a commercial finite element code. The capabilities of the model are demonstrated.

1 Introduction

Traditionally, constitutive models describe the mechanical behavior of materials on a macroscopic level, without a connection to microstructural parameters like grain size or volume fraction of secondary phases. For materials with a wide variation in microstructure or with changing microstructures these models do not yield satisfactory results. The models must be calibrated with experimental results anytime a different microstructure is to be analyzed. Therefore, more recently micro-mechanical models are developed for a wide range of materials, generally following one of two approaches. The first approach is the multi-scale approach in which a direct connection is established between models on the micro and macro level [1,2]. In the second approach detailed models on the micro level are used to develop improved constitutive relations, that can be applied in the traditional macroscopic methods [3,4,5].

Single crystal nickel-base superalloys are widely used as gas turbine blade materials because of their very high resistance against high temperature plastic deformation. The superior high temperature behavior is attributed to the two-phase composite microstructure, consisting of a γ matrix containing a large volume fraction of cuboidal γ' particles (Fig.1a).

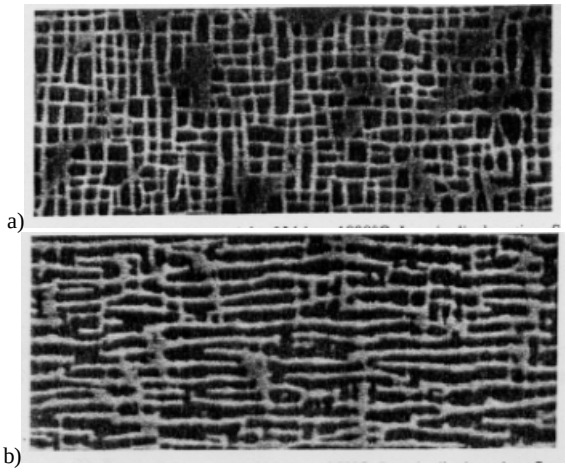

Fig. 1. Micrograph of a Superalloy Microstructure
a. As-Received Condition, b. Ex-Service Condition.

This is a class of materials for which micro-mechanical models are required for two reasons. On the one hand small variations in the alloy heat-treatment can result in different microstructures. On the other hand the microstructure changes considerably during operation at high temperatures. At low stresses the cubic precipitates coarsen and become spherical, whereas under high stresses enlarged and elongated precipitates form (see Fig. 1b.).

To be able to describe the mechanical behavior of these materials and perform reliable life assessments, a multi-scale model was developed [6], as is shown schematically in Fig. 2. The turbine component is modeled on the macro-level as a standard Finite Element (FE)

model. The material microstructure, as a compound of γ and γ' phases is modeled on the meso-level and finally the constitutive behavior of the single phases is modeled on the micro-level.

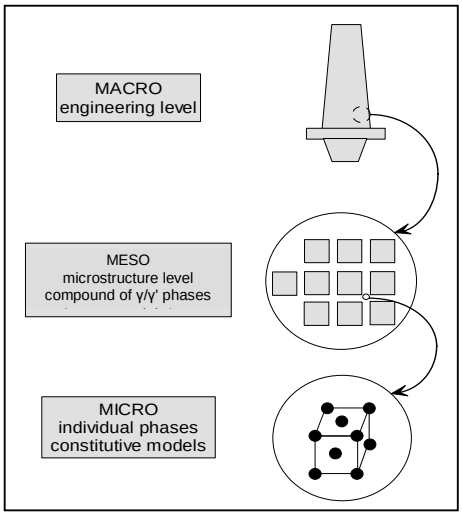

Fig. 2. Schematical Overview of Multi-scale Approach.

2. Multiscale model formulation

Each material point (integration point) on the macro-level is represented by a unit cell on the mesoscopic level, see Fig. 3, which only contains 10 regions. This makes the model computationally efficient in comparison to approaches with global-local FE models. The γ/γ'-interface is believed to have an important effect on the overall material behavior. Therefore, in addition to γ and γ' regions, the unit cell also contains specific interface regions (I_i). The microstructure morphology is defined on this level by choosing the dimensions of the different regions.

The macroscopic deformation of a material point ($\bar{\boldsymbol{\varepsilon}}$) is obtained from the macro-level and by appropriately averaging the resulting deformation of the different regions in the unit cell the material response ($\bar{\boldsymbol{\sigma}}$) is returned to the macro-model.

The mesoscopic strain is obtained by averaging the microstructural quantities in each of the regions, defined as

$$\sum_{i=1}^{N} f^i \boldsymbol{\varepsilon}^i_{tot} = \bar{\boldsymbol{\varepsilon}}_{tot} \qquad i = 1,..,10 \qquad (1)$$

where f^i are the volume fractions, $\boldsymbol{\varepsilon}^i_{tot}$ the total strain tensors in the different regions and N indicates the effective number (10) of regions in the model.

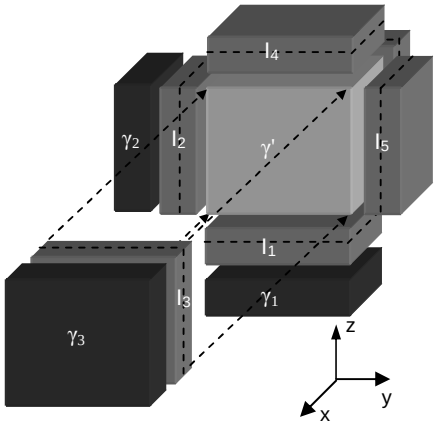

Fig. 3. Schematic Overview of Multi-phase Unit Cell.

The relation between the mesoscopic and microscopic level is provided by the constitutive models, which relate the stress tensors to the individual strain tensors for all 10 regions

$$\boldsymbol{\varepsilon}^i \rightarrow \text{constitutive box} \rightarrow \boldsymbol{\sigma}^i \qquad i = 1,..,10 \qquad (2)$$

The constitutive model on the micro level, for each phase, is based on a strain-gradient enhanced crystal plasticity theory and will be described in section 3.

Inside each of the different regions, both stress and deformation are assumed to be uniform. To specify the coupling between the regions an interaction law has to be defined. Two frequently adopted limit cases can be distinguished:

- Taylor interaction: deformation is uniform across the regions, stresses may vary;
- Sachs interaction: stresses are uniform across the regions, deformation may vary;

These two approaches form an upper and a lower bound for the stiffness, so the real mechanical behaviour intermediates between these cases. A Taylor interaction model is inappropriate for the present application, since

the deformation is highly localized in the γ-matrix phase. A Sachs-type approach is actually a much better approximation, but it lacks the ability to incorporate kinematical compatibility conditions at the interface. Therefore, a modified Sachs approach [7] is used, in which the requirement of a uniform stress state is relaxed for the interface regions. In the γ and γ'-regions the stresses are required to be equal to the mesoscopic stress. In each pair of interface regions however, only the *average* stress is enforced to be equal to the mesoscopic stress. This results in the following equations:

- Sachs interaction between γ' and γ-regions

$$\boldsymbol{\sigma}^{\gamma'} = \boldsymbol{\sigma}^{\gamma_1} = \boldsymbol{\sigma}^{\gamma_2} = \boldsymbol{\sigma}^{\gamma_3} = \bar{\boldsymbol{\sigma}} \qquad (3)$$

- Modified Sachs interaction for the bi-crystal interfaces

$$f^{\mathrm{I}_k^{\mathrm{p}}}\boldsymbol{\sigma}^{\mathrm{I}_k^{\mathrm{p}}} + f^{\mathrm{I}_k^{\mathrm{m}}}\boldsymbol{\sigma}^{\mathrm{I}_k^{\mathrm{m}}} = \left(f^{\mathrm{I}_k^{\mathrm{p}}} + f^{\mathrm{I}_k^{\mathrm{m}}}\right)\bar{\boldsymbol{\sigma}} \qquad k=1,2,3 \qquad (4)$$

where $\boldsymbol{\sigma}^{\mathrm{i}}$ are the stress tensors in the different regions, $\bar{\boldsymbol{\sigma}}$ is the mesoscopic stress tensor and f^i are the volume fractions of the respective regions.

The fact that both partitions of the interface region may respond differently to a mechanical load enables the possibility (and necessity) to define additional conditions at the interfaces. Both stress continuity (across the interface) and kinematical compatibility (in the plane of the interface) are therefore added as additional requirements, where $\vec{n}^k$ is the unit normal vector on the k^{th} interface:

- Compatibility between the matrix $(\mathrm{I}_k^{\mathrm{m}})$ and the precipitate side $(\mathrm{I}_k^{\mathrm{p}})$ of the k^{th} interface:

$$\boldsymbol{\varepsilon}^{\mathrm{I}_k^{\mathrm{p}}} \cdot \left(\mathbf{I} - \vec{n}^k\vec{n}^k\right) = \boldsymbol{\varepsilon}^{\mathrm{I}_k^{\mathrm{m}}} \cdot \left(\mathbf{I} - \vec{n}^k\vec{n}^k\right) \qquad k=1,2,3 \qquad (5)$$

- Stress continuity at the same interface:

$$\boldsymbol{\sigma}^{\mathrm{I}_k^{\mathrm{p}}} \cdot \vec{n}^k = \boldsymbol{\sigma}^{\mathrm{I}_k^{\mathrm{m}}} \cdot \vec{n}^k \qquad k=1,2,3 \qquad (6)$$

where $\boldsymbol{\sigma}$ and $\boldsymbol{\varepsilon}$ are the stress and strain tensors in the different regions.

3. Constitutive behavior

On the micro-level the constitutive behavior of the different phases is described by crystal plasticity models, assuming that the plastic deformation of metals is a natural consequence of the process of crystallographic slip. For each type of crystal lattice a set of slip systems exists along which the slip process will take place. A slip system is commonly characterised by its slip plane and its slip direction. For the considered superalloy, with a face-centred cubic (FCC) lattice, 3 slip directions on each of the 4 octahedral slip planes can be identified, resulting in 12 slip systems. In addition to the plastic slip, elastic deformation is accommodated by distortion of the crystallographic lattice.

Clearly, crystallographic slip is carried by the movement of dislocations. Yet, also the hardening behaviour of metals is attributed to dislocations. Plastic deformation causes multiplication of dislocations and their mutual interaction impedes the motion of gliding dislocations, which causes strengthening. The total dislocation population can be considered to consist of two parts:

- statistically stored dislocations (SSD)
- geometrically necessary dislocations (GND)

The SSDs are randomly oriented and therefore do not have any directional effect and no net Burgers vector. They accumulate through a statistical process. On the other hand, when a gradient in the plastic deformation occurs in the material, a change of the GND density is required to maintain lattice compatibility. Individual dislocations cannot be distinguished as SSDs or GNDs. The GNDs are therefore the fraction of the total dislocation population with a non-zero net Burgers vector. Moreover, as will be shown later, a gradient in the GND density causes an internal stress which affects the plastic deformation.

3.1 Matrix phase constitutive model

The basic ingredient of the crystal plasticity framework is the relation between the

slip rates $\dot{\gamma}^\alpha$ and the resolved shear stresses τ^α for all the slip systems α:

$$\dot{\gamma}^\alpha = \dot{\gamma}_0 \left\{ \frac{\left|\tau^\alpha_{eff}\right|}{s^\alpha} \right\}^m \left\{ 1 - \exp\left(-\frac{\left|\tau^\alpha_{eff}\right|}{\tau^{or}} \right) \right\}^n \text{sign}\left(\tau^\alpha_{eff}\right) \quad (7)$$

where τ^{or} denotes the Orowan stress, s^α the actual slip resistance and τ^α_{eff} the effective stress on slip system α, defined as the combination of the resolved shear stress, the back stress and the misfit stress (see section 4).

$$\tau^\alpha_{eff} = \tau^\alpha + \tau^\alpha_{misfit} - \tau^\alpha_b \quad (8)$$

The resolved shear stress τ^α is obtained by Schmid decomposition of the Cauchy stress tensor $\boldsymbol{\sigma}$ by

$$\tau^\alpha = \boldsymbol{\sigma} : \mathbf{P}^\alpha \quad (9)$$

where $\mathbf{P}^\alpha$ is the symmetric tensor. The (projected) back stress and misfit stress are obtained from the corresponding stress tensors in the same way.

For the present two-phase material, the slip law contains a threshold term for the Orowan stress, which is the stress required to bow a dislocation line into the channel between two precipitates. This stress is given by [8] as

$$\tau^{or} = \frac{\mu b}{2\pi d} \ln\left(\frac{d}{r_0}\right) = \alpha \frac{\mu b}{d} \quad (10)$$

where μ is the shear modulus, b the length of the Burgers vector, d the spacing between two precipitates (equal to the channel width) and r_0 the dislocation core radius (in the order of b).

Slip resistance

The physical mechanism associated with an increasing slip rate at increasing temperature is the decrease of dislocation drag (related to the slip resistance). Slip resistance or dislocation drag is caused by several obstacles like solute atoms, precipitates and other dislocations, each having a contribution to the overall slip resistance. The contribution of dislocations to the slip resistance is related to the availability of mobile dislocations and the resistance of sessile / forest dislocations and therefore depends on the total dislocation density, composed of the SSDs and the GNDs. The temperature dependent relation between the slip resistance and the dislocation density is defined according to

$$s^\alpha = c\mu b \sqrt{\left|\rho^\alpha_{SSD}\right| + \left|\rho^\alpha_{GND}\right|} \exp\left[\frac{Q}{kT}\right] \quad (11)$$

where s^α_0 is the a-thermal slip resistance, Q is an activation energy for overcoming the barriers, k is the Stefan-Boltzmann constant and T the absolute temperature.

This formulation requires the knowledge of all dislocation densities (12 edge dislocation densities for the SSDs and 12 edge and 6 screw dislocation densities for the GNDs). The GND densities can be obtained from the plastic deformation gradients in the material as will be explained in section 4 dealing with the internal stresses. The SSD densities are calculated on the basis of an appropriate evolution equation [9], starting from their initial value $\rho_{SSD,0}$:

$$\dot{\rho}^\alpha_{SSD} = \frac{1}{b}\left(\frac{1}{L^\alpha} - 2y_c \rho^\alpha_{SSD} \right) \left|\dot{\gamma}^\alpha\right| \quad (12)$$

which is the net effect of dislocation accumulation (left term) and annihilation (right term). The parameter y_c represents the critical annihilation length, i.e. the average distance below which two dislocations of opposite sign annihilate spontaneously. The accumulation rate is linked to the average dislocation segment length of mobile dislocations on system α, which is determined by the current dislocation state through

$$L^\alpha = \frac{K}{\sqrt{\left|\rho^\alpha_{SSD}\right| + \left|\rho^\alpha_{GND}\right|}} \quad (13)$$

where K is a material constant.

3.2 Precipitate constitutive model

In the present model, the precipitate in the superalloy is assumed to be elastic. This assumption is only acceptable under certain conditions. The precipitate may deform

inelastically when it is sheared by a dislocation or bypassed by dislocation climb. However, these processes have considerable thresholds in terms of stress and temperature. Therefore, at temperatures below 950 ^{o}C and moderate stress levels the simplification of an elastically deforming precipitate is justified.

4. Internal stresses

The interface between the two different phases plays an important role in the mechanical behaviour of the multi-phase material, because of the development of significant internal stresses that interact with the externally applied stress. In the present model the following internal stresses are incorporated:

- misfit stress: stress that originates from the lattice misfit between the γ and γ'-phases at the level of the coherent interface that is formed.
- back stress: stress that originates from deformation-induced plastic strain-gradients inducing a gradient in the GND density at the interfaces.

These interface effects are only included in the interface regions of the model.

The γ and γ'-phases both have an FCC lattice structure with a slightly different lattice (dimension) parameter. They form a coherent interface, which means that the crystal lattice planes are continuous across the interface, but a misfit strain exists to accommodate the difference in lattice parameter. For most superalloys the misfit is called negative, which means that the lattice parameter of the precipitate is smaller than the matrix lattice parameter. To bridge the misfit, both the precipitate and matrix are strained, causing compressive misfit stresses in the matrix (parallel to the interface) and tensile stresses in the precipitate. These misfit stresses are internal stresses which are consequently zero when averaged over the unit cell.

The amount of straining of the matrix and precipitate is dependent on the magnitude of the misfit, the elastic moduli of both materials and their relative sizes [10]. The unconstrained misfit is defined as

$$\delta = \frac{a_{\gamma'} - a_{\gamma}}{a_{\gamma}} \tag{14}$$

with $a_{\gamma'}$ and a_{γ} the lattice parameters of the γ' and γ-phases respectively. The coefficient of thermal expansion is not equal for both phases, so the misfit is temperature dependent, since the difference in lattice parameter changes with temperature.

The misfit between the two phases can be relaxed by plastic deformation of one or both phases. Plastic deformation generates misfit dislocations at the interface resulting in a loss of coherency between the phases and a corresponding relaxation of the misfit stress.

The back stress on a slip system originates from the spatial distribution of dislocations and is therefore only related to the GND density. For SSDs, which usually have a random orientation, the back stress contribution will be negligible. The value of the back stress tensor is calculated by summation of the internal stress fields caused by the individual edge and screw dislocation densities.

$$\boldsymbol{\sigma}_{\mathbf{b}} = -\left(\boldsymbol{\sigma}_{e}^{\text{int}} + \boldsymbol{\sigma}_{s}^{\text{int}}\right) \tag{15}$$

For a field of edge dislocations the stress field in a point is approximated by summation of the contributions of all dislocation systems ξ in a region with radius R around that point [11], resulting in

$$\boldsymbol{\sigma}_{e}^{\text{int}} = \frac{\mu b R^2}{8(1-\nu)} \sum_{\xi=1}^{12} \vec{\nabla} \rho_{GND}^{\xi} \cdot \left(3\vec{n}^{\xi}\vec{s}^{\xi}\vec{s}^{\xi} - \vec{s}^{\xi}\vec{s}^{\xi}\vec{n}^{\xi} - \vec{s}^{\xi}\vec{n}^{\xi}\vec{s}^{\xi} + \vec{n}^{\xi}\vec{n}^{\xi}\vec{n}^{\xi} + 4\vec{n}^{\xi}\vec{p}^{\xi}\vec{p}^{\xi}\right) \tag{16}$$

where the vectors $\vec{s}$ and $\vec{n}$ are in the direction of the Burgers vector and slip plane normal respectively and $\vec{p}$ is defined as $\vec{p} = \vec{s} \times \vec{n}$, i.e. the dislocation line vector for an edge dislocation.

For the field of screw dislocations the stress field is given by

$$\boldsymbol{\sigma}_{s}^{\text{int}} = \frac{\mu b R^2}{4} \sum_{\xi=13}^{18} \vec{\nabla} \rho_{GND}^{\xi} \cdot \left(-\vec{n}^{\xi}\vec{s}^{\xi}\vec{p}^{\xi} - \vec{n}^{\xi}\vec{p}^{\xi}\vec{s}^{\xi} + \vec{p}^{\xi}\vec{s}^{\xi}\vec{n}^{\xi} + \vec{p}^{\xi}\vec{n}^{\xi}\vec{s}^{\xi}\right) \tag{17}$$

where $\vec{p} = \vec{s} \times \vec{n}$ is now perpendicular to the dislocation line direction (since the Burgers vector is parallel to the dislocation line). Note that only a non-zero gradient of the GND densities causes a non-vanishing contribution.

To calculate the back stress, it is necessary to know the distribution of the dislocation densities for all individual slip systems. These densities can be obtained from the slip gradients in the material. For the edge dislocations (ξ = 1… 12) the GND densities are obtained from the slip gradients by

$$\rho_{GND}^{\xi} = \rho_{GND,0}^{\xi} - \frac{1}{b} \vec{\nabla} \gamma^{\xi} \cdot \vec{s}^{\xi} \qquad (18)$$

and for the screw dislocations (ξ = 13… 18) by

$$\rho_{GND}^{\xi} = \rho_{GND,0}^{\xi} + \frac{1}{b} \left(\vec{\nabla} \gamma^{\alpha_1} \cdot \vec{p}^{\alpha_1} + \vec{\nabla} \gamma^{\alpha_2} \cdot \vec{p}^{\alpha_2} \right) \qquad (19)$$

Since the real deformation distribution in the unit cell is simplified by assuming uniform deformation inside each region, gradients in slip are captured through discrete steps in between regions only.

5. Application

In this section, the capabilities of the model in predicting material behavior and the efficiency of the multi-scale approach are demonstrated. The model was implemented in a user-subroutine in the commercial FE code MSC.Marc and can therefore be applied to any available FE model. Firstly, the effects on the material mechanical behavior of precipitate volume fraction and size are analyzed, using a one-element model. Secondly, the model is applied to a real gas turbine component model.

5.1 Material mechanical behavior

A very simple single element FE model is used to demonstrate the material point response of the multi-scale model by simulating a tensile test at 850 ^{o}C and a strain rate of 3.33x10^{-4} s^{-1}. A microstructure which is typical for the commercial nickel-based superalloy CMSX-4 is used as a reference: cubic precipitates with a size of 500 nm are divided by matrix channels with a width of 60 nm. This yields a precipitate volume fraction of 71%. The calculated tensile curve is shown in Fig. 4. together with an experimentally determined curve, showing that the model can accurately describe the material behavior.

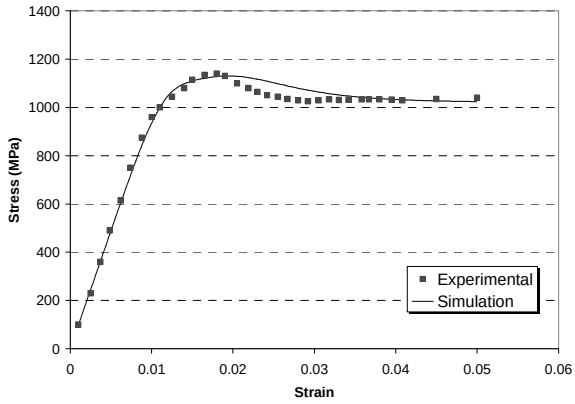

Fig. 4. Simulated stress-strain curve for CMSX-4 at 850^{o}C at a strain rate of 3.33 .10^{-4} s^{-1} compared to an experimentally determined curve.

Applying a different heat treatment or exposing the material to a high temperature for a prolonged period of time can result in a microstructure that differs from the typical (and optimized) microstructure. The present model can be used to study the effects of different morphologies on mechanical behavior. In the following, the effect of changes in precipitate volume fraction and precipitate size will be analyzed.

Firstly the precipitate volume fraction is varied by changing the precipitate size. The matrix channel width is kept constant to exclude the effect of a changing Orowan threshold. Fig. 5. shows the tensile curves for materials with a precipitate volume fraction ranging from 52% to 73%.

Since the material is a compound of two phases, the precipitate volume fraction determines the relative contribution of the precipitate phase to the macroscopic response. The precipitate is treated as an elastic medium and therefore the matrix phase accommodates all plastic deformation. Increasing the precipitate volume fraction decreases the

amount of material available for plastic deformation and therefore increases the yield strength, as can be seen in Fig. 5.

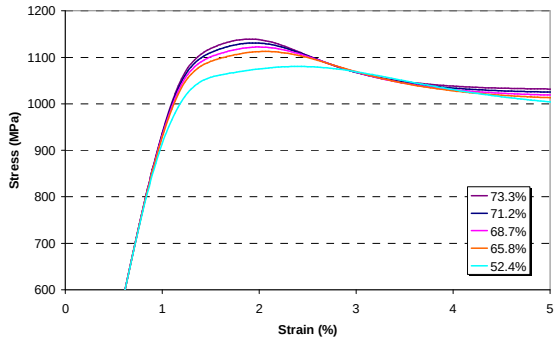

Fig. 5. Effect of changing precipitate volume fraction on the tensile curve.

Secondly, the effect of changing the precipitate size is studied, whilst the volume fractions are kept constant. The latter can only be accomplished when the width of the matrix channels is changed proportionally. The resulting size effects are caused by a combination of two mechanisms:

- decreasing the matrix channel increases the Orowan threshold,
- decreasing the matrix channel increases the deformation gradients in the material and hence the back stresses,

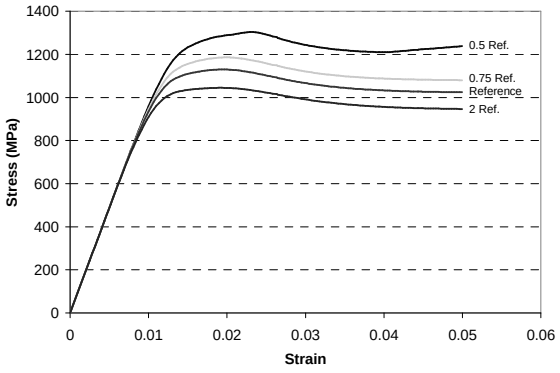

Fig. 6. Effect of changing microstructural dimensions on the tensile curve.

These size effects are shown in Fig. 6., in which the tensile curve for the reference case is compared to the curves for cases with all unit cell dimensions multiplied by a factor 0.5, 0.75 and 2. This shows that increasing the microstructural dimensions causes a decrease in material strength.

Finally, the simulated size effects were compared to experimental results (Fig. 7.). Duhl [12] measured the change of the steady-state flow stress at different precipitate sizes for PWA1480, a similar nickel-based superalloy with a high precipitate volume fraction. The steady-state flow stresses were normalized by the values for the reference cases to enable a direct comparison in Fig. 7. Although the experimental results were determined at 760 ^{o}C and the present model was calibrated for 850 ^{o}C, the observed size effect could be simulated quite well. In the simulations, the steady-state flow stress was defined as the stress level at the end of the curve (at 5 % total strain).

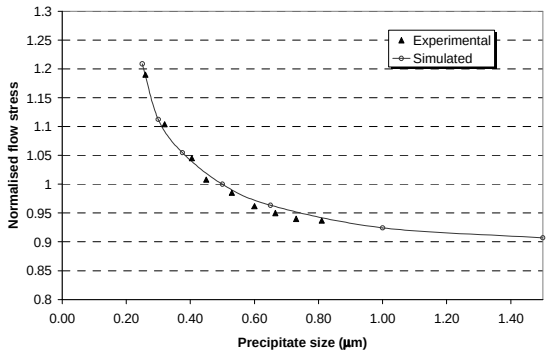

Fig. 7. Effect of changing microstructural dimensions on the steady-state flow stress for CMSX-4 at 850 ^{o}C. Experimental data for PWA1480 at 760 ^{o}C obtained from [12].

5.2 Application to a real component

Due to the efficient multi-scale approach used for the present model, it is possible to analyze the effects of microstructural changes on the macroscopic response of a real gas turbine component. This is demonstrated by application of the model to a low pressure turbine blade FE model. The blade is solid and does not contain any cooling channels. Moreover, it is rotating at a high speed and a pressure difference is applied across the airfoil.

The temperature distribution in the blade and the calculated stress distribution are shown in Fig. 8.

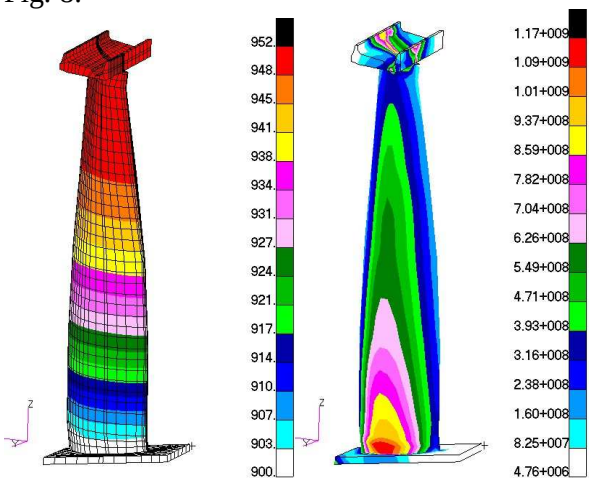

Fig. 8. Temperature (^{o}C) and stress (Pa) distribution in the turbine blade as used for the creep analysis.

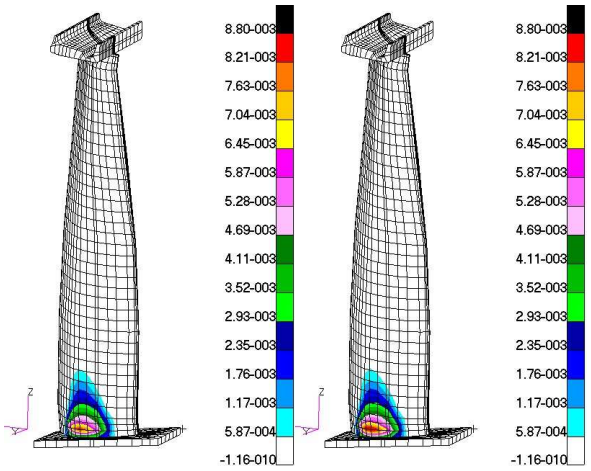

Fig. 9. Creep strain distribution in the turbine blade after a period of time for the reference microstructure (left) and a coarsened microstructure (right).

During operation, the combination of a high metal temperature and considerable stress levels will cause the component to creep at specific locations. The accumulation of creep strain in the blade is calculated by simulating service conditions at a constant speed and temperature.

In the analysis, the presented multi-scale model is used, which means that the unit-cell model (see Fig. 2.) is solved for any material point in the FE model. In this way there is a direct link between micro and macro scale, but still the analysis only takes about half an hour of computation time on a desktop computer. This demonstrates that the presented multi-scale approach is computationally very efficient.

The resulting distribution of creep strain after a certain period of time is shown in Fig. 9. for two different microstructures: the reference case and a coarse microstructure with all microstructural dimensions increased by a factor 2. Comparison of the two plots shows that the creep strain accumulation is faster for the coarse microstructure, which is also illustrated in Fig.10. This figure compares the creep strain accumulation in time at a specific location in the blade for the two microstructures. In the blade with the coarse microstructure the creep strain is 18% higher than in the blade with the reference microstructure.

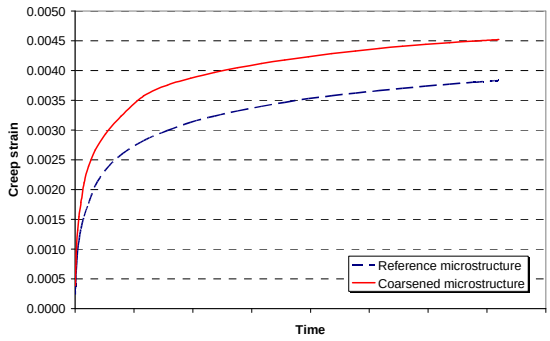

Fig. 10. Comparison of the creep strain accumulation in at a position in the root of the blade for the two different microstructures.

This strong influence of the microstructure on the macroscopic response of components illustrates the relevance of the presented micro-mechanical model. As small variations in the alloy heat-treatment can result in different microstructures, the present model can be used to assess the effects on alloy performance. Also, since the microstructure changes considerably during operation at high temperatures, using the initial microstructure and associated mechanical properties for design or lifing purposes might not be very useful. When the changes in microstructure during service are known, the present model can be used to perform a life

assessment with the actual mechanical properties.

6. Conclusions

A computationally efficient multi-scale micro-mechanical model for a nickel-base superalloy is presented. The model takes into account the multiphase character of the material and is thus able to predict the effect of microstructure morphology on the macroscopic material response. This was illustrated by analyzing the effect of precipitate volume fraction and size on the material tensile behavior. The efficiency of the model was demonstrated by the application to a complex FE model of a real gas turbine component.

7. Acknowledgements

The authors want to acknowledge the Dutch Ministry of Defence for funding part of this research under contract NTP N02/12.

References

[1] Fedelich, B. A microstructural model for the monotonic and the cyclic mechanical behavior of single crystals of superalloys at high temperatures. *International Journal of Plasticity*, 18, 1-49,2002.

[2] Fedelich, B. A microstructure based constitutive model for the mechanical behavior at high temperatures of nickel-base single crystal superalloys. *Computational Materials Science*, 16, 248-258,1999.

[3] Busso, E. P., Meissonnier, F. T., and O'Dowd, N. P. Gradient-dependent visco-plastic deformation of two-phase single crystals. *Journal of the Mechanics and Physics of Solids*, 48, 2333-2361,2000.

[4] Svoboda, J. and Lukas, P. Creep deformation modelling of superalloy single crystals. *Acta Materialia*, 48, 2519-2528,2000.

[5] Choi, Y. S., Parthasarathy, T. A., and Dimiduk, D. M. Numerical study of the flow responses and the geometric constraint effects in Ni-base two-phase single crystals using strain gradient plasticity. *Materials Science and Engineering A*, 397, 69-83,2005.

[6] Tinga, T., Brekelmans, W. A. M., and Geers, M. G. D. A strain-gradient crystal plasticity framework for single crystal nickel-based superalloys. *Journal of the Mechanics and Physics of Solids*, submitted, 2006.

[7] Evers, L. P., Parks, D. M., Brekelmans, W. A. M., and Geers, M. G. D. Crystal plasticity model with enhanced hardening by geometrically necessary dislocation accumulation. *Journal of the Mechanics and Physics of Solids*, 50, 2403-2424,2002.

[8] Yuan, C., Guo, J. T., and Yang, H. C. Deformation mechanism for high temperature creep of a directionally solidified nickel-base superalloy. *Scripta Materialia*, 39, 991-997,1998.

[9] Evers, L. P., Brekelmans, W. A. M., and Geers, M. G. D. Non-local crystal plasticity model with intrinsic SSD and GND effects. *Journal of the Mechanics and Physics of Solids*, 52, 2379-2401,2004.

[10] Porter, D. A. and Easterling, K. E. *Phase transformations in metals and alloys*. Chapman & Hall, London, UK, 1992.

[11] Bayley, C. J., Brekelmans, W. A. M., and Geers, M. G. D. A comparison of dislocation induced back stress formulations in strain gradient crystal plasticity. *International Journal of Solids and Structures*, submitted, 1-27,2005.

[12] Duhl, D. N. Directionally solidified superalloys. in *Superalloys II: High temperature materials for aerospace and industrial power*, Sims, C. T., Stoloff, N. S., and Hagel, W. C., John Wiley and Sons Ltd, New York, 1987.